USE OF SINTERED BAUXITE SAND IN BINDER JETTING OF CASTING CORES

Patricia Erhard, Carla Reddersen, Lucas van den Bosch and Daniel Günther
Fraunhofer Institute for Casting, Composite and Processing Technology IGCV, Lichtenbergstrasse 15, 85748 Garching, Germany

Peter Miura Nakachima, André Luis Pereira, Santiago Maya Johnson and Luis Leonardo Horne Curimbaba Ferreira
Mineração Curimbaba Ltda, Av. João Pinheiro 3665, Poços de Caldas 37701-387, Brazil

https://doi.org/10.1007/s40962-025-01691-8

Abstract

In this article, the processing of sintered bauxite sand with a high aluminum oxide content in 3D printing of casting molds and cores with furan resin is investigated regarding the performance achievable with this material system that is tailored for foundry applications. Suitable parameters for processing in a commercial binder jetting system, VX500, were identified. The influence of the binder and catalyst content as well as the coating speed on the properties of 3-point bending strength, surface roughness, and gas permeability is shown and compared with the most used quartz sand system, GS14 RP. Finally, a benchmark geometry to assess the 3D sand printing shape details and a demonstration geometry that is demanding in terms of core removal are produced. The effect of the molding material system on the surface quality of an aluminum casting is quantified. It was found that an increased catalyst content is required to process the bauxite sand in furan 3D printing. Due to its high flowability, this can be added to the sand without any detrimental effects on the coating speed. Indeed, the coating speed could be doubled compared to the silica sand system while the impact of increased catalyst amounts on the resulting emissions needs to be examined. With the bauxite sand, 3-point bending strengths of above 3 MPa and gas permeability of higher than 300 could be achieved with suitable 3D printing process parameters at mean roughness depths R_z of approximately 170 µm, resulting in a roughness R_z on the order of 110 µm in the casting. The specific advantages of the bauxite-based ceramic sand, such as low thermal expansion, high sphericity, and proper refractoriness, could be further exploited in 3D-printed cores for advanced ferrous alloys casting applications.

Keywords: *casting molds, foundry sands, aluminum oxide, 3D printing, sand core making process, multi-step additive manufacturing*

Introduction

Casting technology is recognized for its capability to produce complex parts economically, making this process vital for series production.[1] 3D printing of sand molds offers a way to incorporate the flexibility of additive manufacturing into traditional production methods.[2] Integrating 3D sand printing into traditional foundries can enhance their capabilities for low-volume production and complex castings without significant upfront investment while allowing continued mass production and promoting a seamlessly integrated digital ecosystem.[3]

The properties of casting molds and cores significantly influence the characteristics of the cast parts, particularly near the surface. The different types of sand that are traditionally used in foundries can be divided into natural sands, such as silica, chromite, zircon, or olivine sand, and ceramic sands, one of which is bauxite-based sintered sand. Natural quartz sands are commonly utilized in foundries for their cost-effectiveness, but they face technological challenges like casting defects due to quartz inversion or hindered thermal diffusivity.[4,5] Additionally, the use of

Received: 07 March 2025 / Accepted: 07 June 2025
Published online: 07 July 2025

crystalline silica is becoming increasingly restricted in several regions of the world due to the health risks it entails.[6–9] Sands such as chromite or zirconite do not present these problems and have a low coefficient of expansion and high thermal conductivity;[10] however, their sub-angular grain morphology and wide grain size distribution decrease their potential for use in 3D printing. Bauxite-based sintered sands exhibit a low coefficient of thermal expansion, high mechanical strength and reclamation rate, spherical morphology, and a narrow, easily controllable grain size distribution, owing to their specialized production process.[11,12] For this reason, they are an interesting alternative to be used in 3D printing.[13] Bauxite is traditionally named aluminum ore, since it is composed primarily of aluminum hydroxides. The quality of the ore and the type and amount of the aluminum and other minority minerals establish the end use for the bauxite, also the right process required to produce the technology of the desired application.[14]

Binder jetting technology has the capability to handle a wide variety of powdered materials with the restriction that they must be flowable.[15] The following steps are involved in the binder jetting process: First, the build platform descends by a predetermined layer thickness. The gap created between the underlying layer and the recoater is subsequently filled with powder. Subsequently, a binder is selectively deposited onto the new layer by an inkjet printhead. This binder joins the particles that form the specific cross section of the component being printed and merges it with the print on the layer beneath. These process steps are reiterated until the print job's total height is achieved. The characteristics of the particle material, including their size distribution and shape, significantly impact the flowability of powders and the resulting packing density.[16,17] A further important factor influencing the flowability is the powder's moisture content.[18] Even though relationships between multiple influencing powder characteristics and flow properties are complex and cannot be described analytically, basic statements on the improvement of flowability of powders that are highly relevant for qualifying new materials for use in binder jetting are feasible: Coarse and spherical powders with a preferably narrow PSD (particle size distribution) and a smooth particle surface are easier to process due to flowability reasons. However, any moisture inside the particle material will impede flowability due to the adhesive interparticle forces originating from liquid bridges.[19] Processing well-flowable powders is not only beneficial in terms of increasing the powder bed's packing density, but to be able to increase recoating speeds, thus improving cycle times and processing costs.[15,20]

This study aims to explore the processing of sintered bauxite sand in 3D printing of casting molds and cores using furan resin. By determining processing parameters for the commercial binder jetting system VX500 (voxeljet AG, Germany) and assessing the effects of binder and catalyst content on the mold's material properties relevant for the powder material's utilization in foundries, its manufacturing performance and potential for future applications in casting are assessed. The process chain, encompassing 3D printing, aluminum casting, and decoring, was demonstrated using a pump housing as a demonstration geometry.

Materials and Methods

Binder Jetting Machine

The binder jetting additive manufacturing machine VX500 (voxeljet AG, Friedberg, Germany) used in this work can process PMMA polymer powders, sand, or ceramics. The box volume is 500 mm (x) × 400 mm (y) in area with a maximum depth of 300 mm (z-direction). The layer height is adjustable and depends on the material system used. The machine is equipped with an automatic feeding system that fills the granular material in the recoating unit. For each layer, the recoater deposits the material over a slit opening and flattens the layer with a single blade. The recoater is vibrating during this process. In the printing phase, the print head travels over the build area in multiple passes, each one along the x-axis, perpendicular to the recoating direction. The machine used for the experiments in this work uses an industrial inkjet print head with 360 dpi resolution with all nozzle rows parallel to the y-direction. This print head supports grayscale printing, but in this work, only one waveform for stable droplet deposition was chosen. Different binder contents in the parts were realized by periodic dense pixel patterns of the reduced densities, see Figure 1. In inkjet printing, the waveform or the absolute print head voltage can be changed to adjust the binder content alternatively to this approach. However,

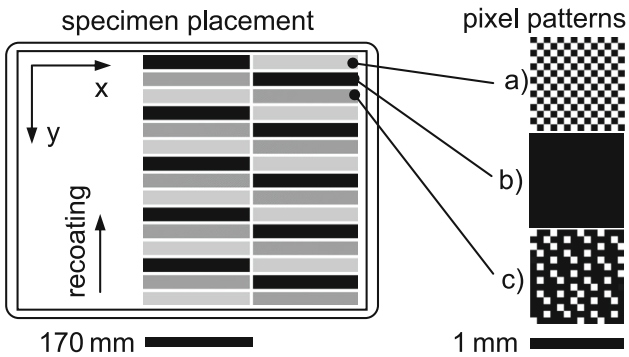

Figure 1. Specimen layout inside build area of voxeljet VX500 machine and detail view of pixel patterns to realize different effective binder concentrations. (a) 50 % pixel density (255 dpi resolution) resulting in 50% binder amount, (b) 100 % pixel density (360 dpi) for maximum binder amount, (c) 75 % density (308 dpi) resulting in 75% binder amount.

those measures lead to a changed energy input into the piezo elements for droplet formation. By keeping the inkjet parameters constant and only varying the resolution, it is estimated that the greatest possible stability of the print result can be achieved.

Molding Materials

Bauxite-based sintered sand was produced by grinding the ore, then agglomerating the fine particles into spheres of desired sizes, and finally sintering them in a rotary kiln at high temperatures. This process results in a dense aggregate with high chemical stability and mechanical strength. The sintering process stabilizes the corundum (alpha-alumina) as major phase. Although the bauxite contains silicon in its composition, it forms a mullite phase or is part of an amorphous material with other oxides, ensuring the absence of free crystalline silica. Furthermore, the production process of this ceramic sand ensures that the grains have a uniform size (with a mean diameter of 0.21 mm) and morphology, guaranteeing greater sphericity and roundness compared to natural sands. Since the silica sand GS14 RP (Strobel Quarzsand GmbH, Freihung, Germany) is the most widely used in the sand 3D printing industry, it was chosen as the benchmark for this study to compare its overall performance. It consists of > 99 % silica with a loss on ignition of < 0.2 %. The particles have an oval, angular shape and appear white with high transparency. The manufacturer gives a mean particle size of 0.13 mm.[21] The properties of both sands can be seen in Table 1. One important feature of the sintered bauxite with regard to the conceivable use of both materials is that it can be magnetized, so that magnetic separation of the molding materials after casting is conceivable.

Both sand materials were stored at room temperature and before filling into the machine, the sands that were used in the grain size distribution as delivered by the suppliers without further sieving were mixed with a catalyst that is based on p-toluene sulfonic acid. The binder is mainly furfuryl alcohol. Both have the trade name RPT2 and were supplied by Hüttenes-Albertus Chemische Werke GmbH (Düsseldorf, Germany).

Experimental Design

The experimental study systematically investigates the effects of binder content, catalyst content, and recoating speed on the material properties of 3D-printed casting molds and cores with sintered bauxite sand, and compares those with 3D-printed silica sand using primarily bending strength specimens (22.4 mm × 22.4 mm × 172 mm). The mold fabrication process involves bonding of the silica or sintered bauxite sand without a subsequent temperature treatment (green part sintering). Since the specimens are fabricated using a no-bake binder system, they are stored at ambient conditions over 24h before material characterization or casting. The layer height is chosen to be 0.28 mm which is a common standard for 3D sand printing with GS14 silica sand. The binder and catalyst content are chosen in relation to known standard processing parameters for silica sand 3D printing according to Table 2 with level 1 corresponding to 2 wt.-% of the weight of silica sand or—due to the higher particle density—1.42 wt.-% of bauxite sand. The lower imprinted binder quantity equals two-thirds of the standard, and the higher quantity is four-thirds of the standard amount. This approach ensures that exactly the same print head settings (resolution, print head

Table 1. Physicochemical, Mechanical (at Room Temperature), and Thermal Properties (at 600°C) of the Foundry Sands

Sand type	Sintered Bauxite	Silica
Source	Brazil	Germany
Process	Ceramic processing	Natural aggregate
Product name	CastBall AFS 65 Premium 3D	GS14 RP
AFS classification	65	97[21]
Bulk density in g/cm^3	2.12	1.32[21]
Particle density in g/cm^3	3.73	2.65
Thermal expansion in %	0.019	1.2[10]
Specific heat capacity, C_p in J/(g K)	0.460	1.25[22]
Thermal conductivity in W/(m K)	0.407	0.345[10]
Chemical Composition (wt.-%)		
Al2O3	73.00	0.2[21]
SiO2	7.32	99.1[21]
Fe2O3	14.40	0.1[21]
TiO2	2.43	0.2[21]
Others	2.85	0.4[21]

Table 2. Material and Process Parameters

Sand type	Binder content	Catalyst content in wt.-%	Recoating speed in mm/s
Sintered bauxite	2/3 (low), 1 (medium), 4/3 (high)	0.2, 0.3, 0.4	100, 200, 400
Silica sand	2/3 (low), 1 (medium), 4/3 (high)	0.2	100

voltage, waveform, droplet sizes, and printing frequency) can be used for the production of specimens for both material systems. For research purposes, the VX500 3D printing system was manipulated to be able to print the three different binder contents simultaneously in only one print job. This offers advantages in terms of comparability and the testing effort. The factor levels of the parameter catalyst content are set to 0.2, 0.3, and 0.4 wt.-% when printing sintered bauxite as a consequence of preliminary tests which showed that an increased amount of catalyst is required for bauxite sand. The recoating speed was initially varied between 100, 200, and 400 mm/s for the medium catalyst content of 0.3 % and kept constant at 200 % for further investigations on the interaction between binder and catalyst amount. For comparison with the silica sand material system that is already established on the market, a catalyst content of 0.2 wt.-% and a recoating speed of 100 mm/s is used. Due to the poorer flowability of the silica sand, it was not possible to increase the speed or catalyst content of this material system using the 3D printing machine as described above.

Relationships between the 3D printing parameters and the mold properties are visualized in box plots showing exclusive interquartile ranges or bar charts with scatter bars. The number of specimens n is specified in each diagram's caption as an absolute number or an interval. Any data points outside the whiskers are considered outliers and represented as individual points.

Once suitable printing parameters were found, the 3Dbenchy as a standardized computer model designed for benchmarking additive manufacturing processes was printed. Aluminum castings encasing bending bar specimens and casting of a pump housings as demonstration geometry were carried out using a printed core made of bauxite sand and one made of quartz sand.

Material Characterization

Particle Analysis

Both silica sand and bauxite-based sintered sand were analyzed optically by the PartAn 3D particle analyzer machine shown in Figure 2. For this, a sample of the materials was taken from their containers, making sure to collect a representative aliquot, with the proportional amount of fines and coarse particles. Each sample was allowed to run fully through the particle analyzer, as fine content tends to pool toward later times.

Light Microscopy

Micrographs were captured using the BX53M microscope (Olympus Europa SE & Co. KG, Hamburg, Germany).

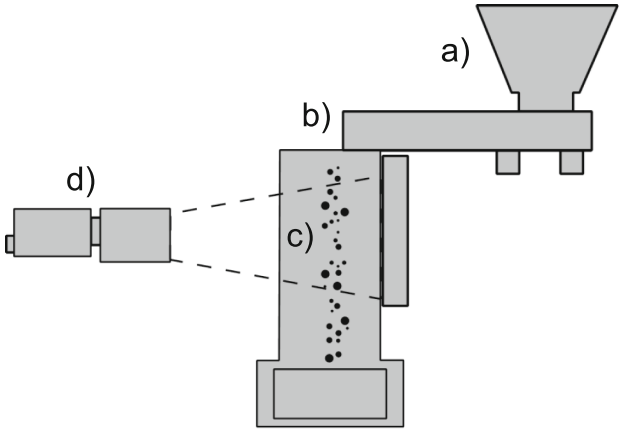

Figure 2. Schematic diagram of the PartAn 3D optical particle analyzer. Granulates are filled into a funnel (a) and transported along a vibrating channel (b). At the end of this channel, granulates fall freely (c) in front of a light screen where they are captured by a high-speed camera (d) for image analysis.

3-Point Bending Strength

In accordance with BDG P72 guideline, 3-point bending testing was conducted on the universal testing machine Z020 (ZwickRoell GmbH & Co. KG, Ulm, Germany) using a 20 kN load cell and a support distance of 150 mm. A number n of five specimens with a cross section of 22.4 mm × 22.4 mm and a total length of 172 mm were tested for every parameter set.

Abrasion Resistance

For characterizing abrasion resistance, the Simpson scratch hardness tester (Simpson Technologies, Naperville, USA) was used. Measurements were carried out at the same point of each 3D-printed 3-point bending strength sample at the lateral end. For each binder content, four measurements were taken. The results obtained by the testing device are expressed in a dimensionless number according to the "B scale." Since the number is unitless, it is not possible to directly compare the results with those from other experimental setups that may use different scales.

Gas Permeability

Gas permeability which is a number specifying the amount of air passing through a sand specimen was measured in accordance with BDG P41 guideline using the Digital Absolute Permmeter (Model 42105, Simpson Technologies, Naperville, USA) following AFS 5224-13-S standards.[23] Cylindrical samples with a diameter of 50 mm and a height of 50 mm were used for the measurements.

Surface Roughness

The surface roughness was measured using the SJ-410 surface measuring instrument (Mitutoyo Corporation, Kawasaki, Japan). The surface roughness parameters of the cubic samples were measured in the plane perpendicular to the build direction. In the evaluation, only the mean roughness depth R_z is considered to make a statement about the surface roughness. Furthermore, the surface roughness of aluminum cast parts was measured with the same method at the contact plane.

Results and Discussion

Sand Characterization

Both silica and bauxite-based sintered sands were analyzed regarding particle sizes and particle roundness parameters. Figure 3 shows the measurements of the relative and cumulative mass fractions over the sieve number for the sintered bauxite sand "CastBall" and the silica sand "GS14." There is a significant difference in the particle size distribution PSD, with CastBall being significantly coarser and having a narrower PSD compared to GS14 RP. Additionally, the fines content (equivalent to the particles passing through the 230 mesh sieve) was found to be as low as 0.2 % for CastBall while GS14 RP showed approx. 0.5 % fines content by that definition. The larger particle sizes, the reduced fines content, and the narrower particle size distribution resulted in improved flowability and are expected to lead to less binder consumption.

The particle shape parameters shown in Figure 4 exhibit a clear difference between CastBall and silica sand GS14 RP. All values are closer to a perfect sphere for the CastBall, especially for the larger particles (low sieve number). The microscopy images in Figure 5 confirm this assessment. Rounder particles lead to improved flowability in processing and potentially less abrasion of the surfaces in contact with the granulates.

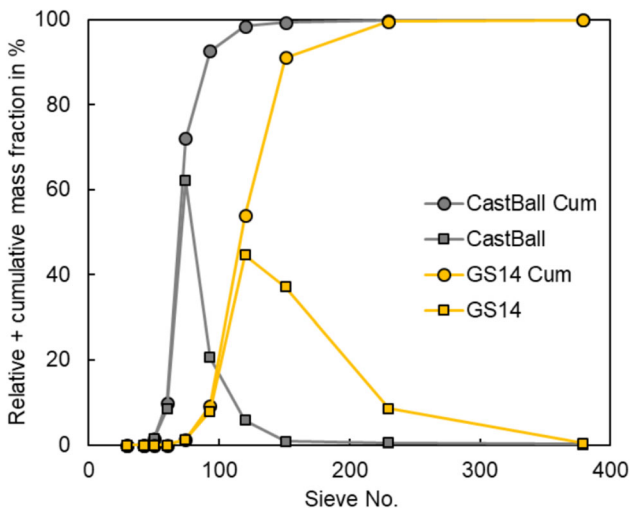

Figure 3. Relative and cumulative particle mass fractions over sieve number (ASTM E11-15) for CastBall and the reference GS14 RP.

3D Printing Processing Parameters

In this chapter, suitable material and process parameters for processing sintered bauxite sand in an industrial binder jetting machine are investigated by analyzing the effect of the recoating speed, binder content, and catalyst content on the 3-point bending strength.

Due to the comparatively rounder shape, and coarser particle size distribution, the bauxite sand system is observed to be highly flowable. Thus, **recoating speeds** as high as 400 mm/s are feasible for processing the artificial sand system with the printing hardware used. In contrast, recoating tests with the silica sand system GS14 RP showed that the recoating speed should not exceed 100 mm/s; otherwise, macroscopic defects would become visible during recoating.

Figure 6 shows the flexural strength distribution achieved when printing bauxite sand mixed with 0.3 wt.-% catalyst with different binder amounts at recoating speeds between 100 and 400 mm/s. The average 3-point bending strength is shown to be highest at 200 mm/s for all levels of binder content. This is remarkable since lower velocities are usually favorable in binder jetting because the particles can arrange themselves more easily into a homogeneous network so that the probability of larger defects occurring in the layer is reduced.[24,25] With a recoating speed of 200 mm/s, an absolute 3-point bending strength of 2.3 MPa on average is found for the medium binder content, an increase of binder by 1/3 only achieves further strength development to around 2.5 MPa. The difference between the binder contents is found greater at the other speeds. This effect could be due to the fact that at the most suitable speed; the sand is compacted so homogeneously that the binder can spread well.

It can be noted that even at a recoating velocity of 400 mm/s—which means a highly productive layer deposition process—still high strength can be observed. Thus, depending on the requirements, one may decide between shorter production times or higher strength of casting cores produced with this hardware, process, and materials.

The standard recipe recommends adding 2 wt.-% furfuryl alcohol binder to silica sand premixed with 0.3 wt.-% catalyst.[26] The lowest catalyst amount 0.2 wt.-% selected for this study is a conversion of this recipe to the higher density of sintered bauxite. Without the addition of additives, the sintered bauxite sand used has a pH value of 7.1

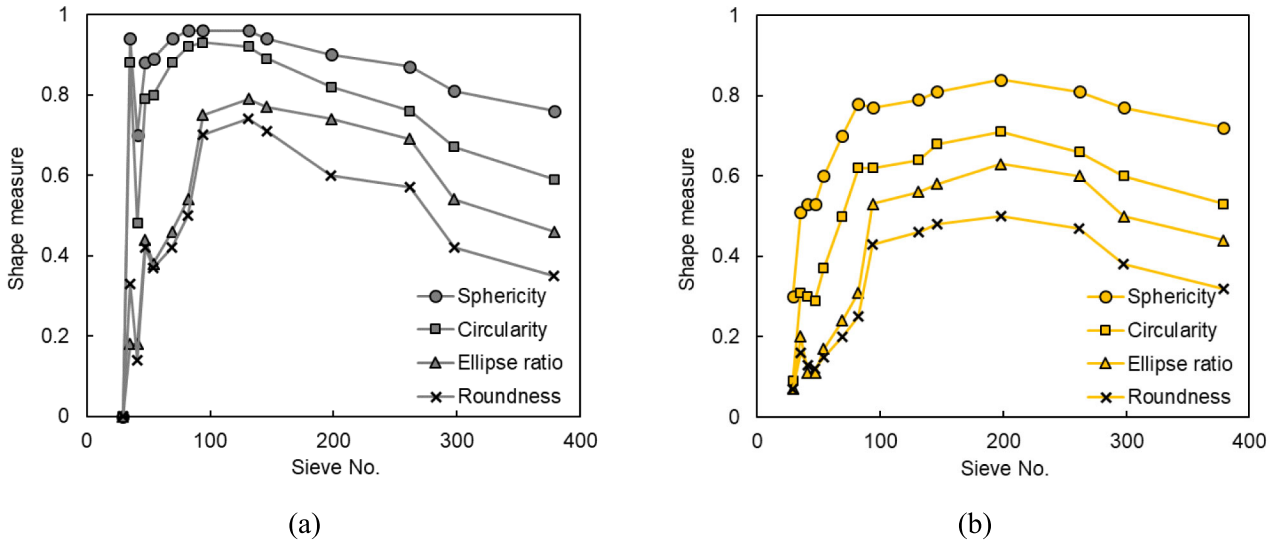

Figure 4. Shape measures of both sand materials (a) CastBall and (b) GS14 RP, analyzed by PartAn 3D. All shape parameters are normalized to be between 0 and 1 (= perfect sphere) and use PartAn 3D definitions.

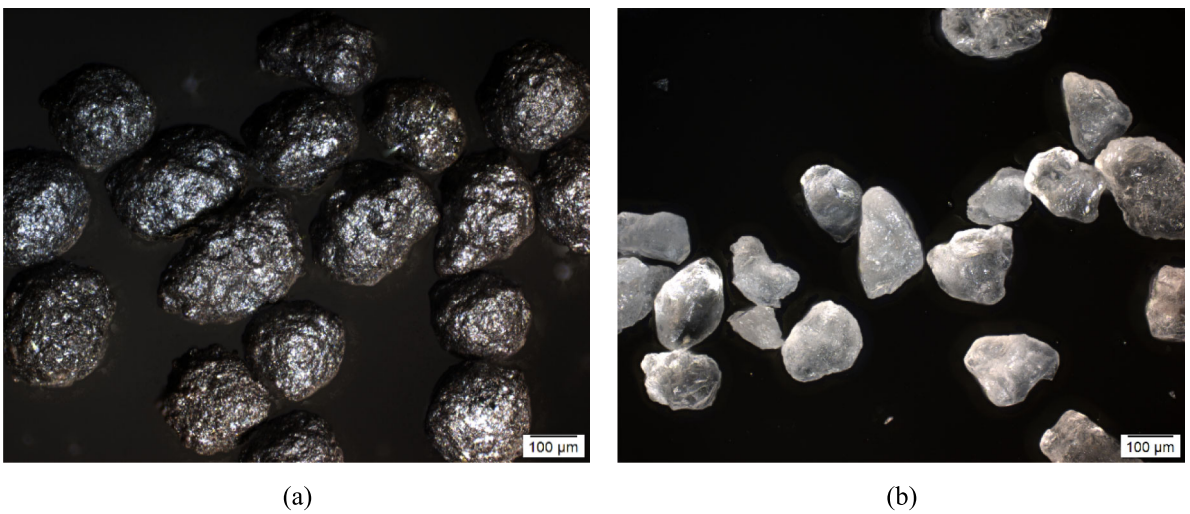

Figure 5. Microscopy photographs of both materials (a) sintered bauxite sand CastBall and (b) silica sand GS14 RP.

while 6.3 was reported for GS14 RP.[27] Due to this, it is expected that a higher amount of acid is required to provide the optimum **catalyst amount** for the reaction with furfuryl alcohol. However, the quantity of liquid bridges in the sand that is impeding the originally good flowability rises by increasing the catalyst amount. The recoating speed is set to 200 mm/s based on the results. A reciprocal influence of the recoating speed and catalyst amount on the absolute bending strength is considered possible for flowability reasons, but is not regarded as decisive when investigating the interaction between binder and catalyst quantity. The processability of sintered bauxite sand after mixing with 0.4 wt.-% catalyst is impaired, but recoating at this velocity is still possible without creating visible layering flaws whereas an increase in the proportion of quartz sand is not possible due to the already lower flowability in the dry state.

Figure 7 illustrates the strength distribution obtained by printing bauxite sand mixed with varying amounts of catalyst, using a recoating speed of 200 mm/s. It is evident that to achieve the most effective strength results, the binder quantity must be precisely adjusted to the catalyst amount. At only 0.2 wt.-% of catalyst, the maximum strength of around 0.9 MPa was achieved with the lowest binder amount, reduced to 0.5 MPa with the standard binder amount, and dropped to 0.4 MPa using the highest binder amount. With a catalyst amount of 0.3 wt.-% the relationship reverses and the additional binder provided can contribute to the strength of the 3D-printed body. At 0.3 wt.-% of catalyst, there was not yet a clear advantage in

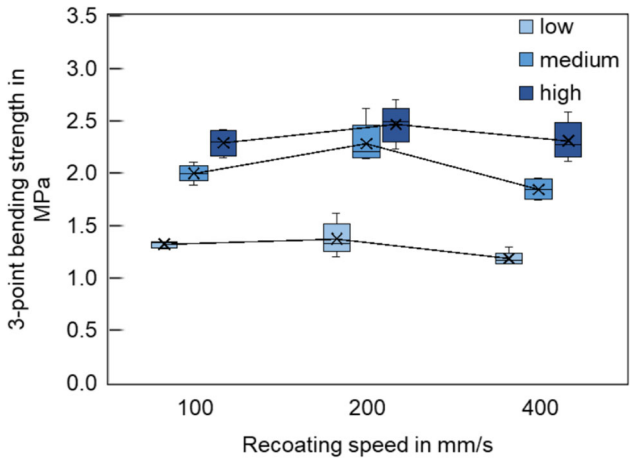

Figure 6. Effect of the recoating speed on the 3-point bending strength of sintered bauxite specimens, with data presented for low, medium, and high binder content. The sintered bauxite sand was mixed with 0.3 wt.-% catalyst immediately before starting the print job. Number of samples n=[4;5].

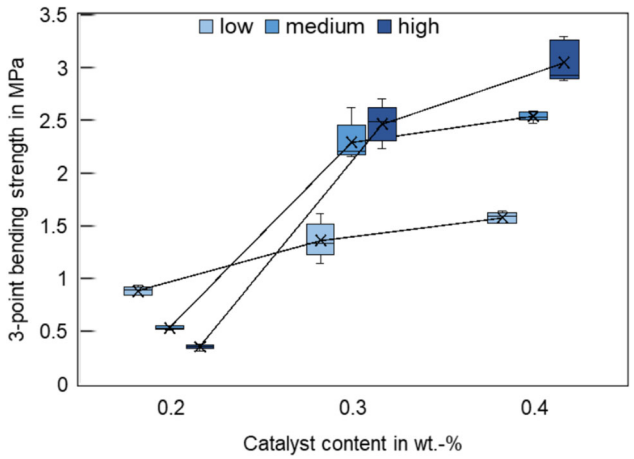

Figure 7. Effect of the catalyst content on the 3-point bending strength of sintered bauxite specimens at a recoating speed of 200 mm/s, with data presented for low, medium, and high binder content. The sintered bauxite sand was mixed with the respective catalyst amount immediately before starting the print job. Number of samples n=5.

terms of strength when using 1/3 more binder (2.5 MPa) than the standard amount (2.3 MPa) but a significant increase in strength compared to the lowest binder amount. However, at a catalyst content of 0.4 wt.-% the bending strength considerably increased to 3 MPa on average when using the highest level of binder. These results comply well with the findings of Son et al. that showed a function between the flexural strength of silica sand specimens bond with furan binder in dependence of the catalyst amount used. For a binder proportion of 2 wt.-%, they observed saturation in strength development from 0.25 wt.-% catalyst. A higher amount of catalyst was found to lead to faster polymerization, more conjugated oligomer sequences, and a darker color, but not stronger binder bridges. However, at 0.25 wt.-% catalyst, the flexural strength was explored to improve further with the additional binder, indicating that here the binder was the limiting factor.[28] In Figures 6 and 7, the scatter seems to be higher at higher strengths. It is assumed that absolute strength variation increases with higher strength, while the percentage value remains at the same level. Future studies should have a higher sample size to trace the variabilities and their origins.

By further increasing the binder and catalyst amount simultaneously, the achievable strength can be further increased. However, the sintered bauxite investigated in this study has a favorable material-specific starting point in terms of flowability but the same challenges connected to impeded flowability as can be observed when printing fine-grained sands will appear. However, it is conceivable that with the material system and adequate hardware, the amount of catalyst can be further augmented, resulting in strengths exceeding 3 MPa. The gas permeability will remain high; however, the generation of noxious gases will increase.

Anwar et al. compared different sand and binder systems with regard to sand core properties relevant for casting and found silica sand as best compatible with the furan binder concerning strength development, followed by zircon and chromite sands. Bauxite sand and Cerabeads were found to not achieve sufficient strength when using a standard catalyst quantity. The authors suspect that this could be due to the pH value and increasing the catalyst amount may be a way to improve strength.[29] In this work, it was shown that the adjustment of the amount of acid provided to the binder quantity dosed through the print head is indeed decisive for the processing of bauxite sand using furan binder (Figure 7). Assuming a similar theoretical bulk density, the absolute quantity of the catalyst is nearly doubled compared to the silica material system. The non-acid character of the bauxite sand could be considered an argument in favor of using alkaline binders, such as sodium silicate, given that excessive addition of sulfonic acid is undesirable in terms of the working conditions in foundries. One advantage of foundry silicate binders is that the strength can be achieved purely by increasing the binder content without the need to adjust a second component that will show interactions with the flowability.[30] As the round-shaped sand can be decored more easily, bauxite sand and water glass binder may be used to produce potentially high-strength filigree hollow structures in advanced cast components.

However, no previous work known by the authors demonstrated the feasibility of using bauxite sand in binder jetting, with the most widely used and extremely reliable printable furan binder. The benchmark geometry 3DBenchy provides a standard for evaluating the capability of additive manufacturing techniques for the manufacture of

Figure 8. Illustration of a #3DBenchy model printed with sintered bauxite sand.

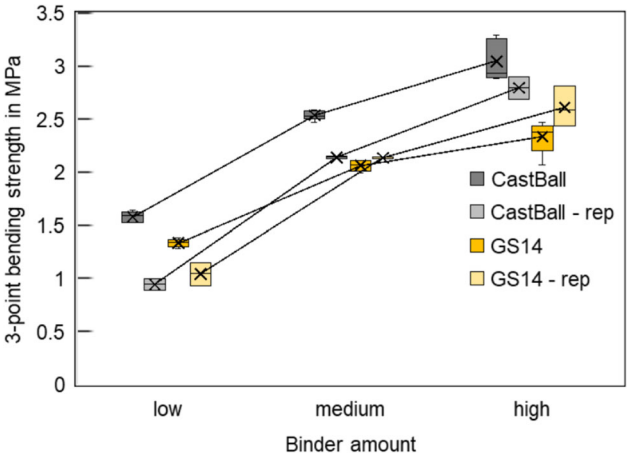

Figure 9. Comparison of the 3-point bending strength achieved during two experimental runs of CastBall premixed with a catalyst amount of 0.4 wt.-% and recoated at a recoating speed of 200 mm/s, and GS14 RP premixed with 0.2 wt.-% catalyst and recoated with 100 mm/s. Number of samples for a repetition of the experiment (ending "-rep") n=[2;3], other n=5.

different geometrical features.[31] The application of the parameter sets developed in this study demonstrates the viability of feature sizes of 3 mm (Figure 8, chimney hole), despite the use of relatively coarse raw materials.

Benchmark of the Mold Properties

Figure 9 compares the **3-point bending strength** achieved when processing sintered bauxite sand premixed with 0.4 wt.-% binder at a recoating speed of 200 mm/s as a parameter set with great potential for producing high-strength sand molds and cores with the reference material silica sand GS14 RP that is premixed with 0.2 wt.-% catalyst and recoated at 100 mm/s. It was found that the recommended catalyst amount of 0.3 wt.-% cannot be used due to the cohesive behavior that leads to excessive macroscopic flaw generation when using the available VX500 recoater setup and faster recoating is difficult for the same reason. In Figure 9, two print jobs using the same parameter set are compared for reproducibility evaluation. Although it was ensured that the drop mass of the print head was identical before each job, major deviations in bending strength between two identical print jobs were found when processing both materials. This could have some reasons: The homogenization status after mixing with catalyst cannot be measured, so it could be that different amounts of catalyst are present locally that were found to significantly influence the final bending strength. Another explanation would be the relatively high probability of the formation of layer defects when printing highly cohesive and poorly flowable powders. A statistical distribution of flaws may therefore be reflected in the measurable bending strengths. A third reason could be environmental factors, in particular fluctuations in temperature and humidity during printing and curing.

In Figure 9, the impression can arise that CastBall has a higher variability. However, the reason are higher absolute variations with higher strength while the proportionate variation remains comparable as it was also within the data sets for 3D-printed bauxite sand (Figures 6 and 7).

Despite a high variation within the data, it is shown that with a sufficiently higher addition of catalyst sintered bauxite sand can be processed in furan sand 3D printing. The observations from preliminary studies about strength formation align well with the results shown herein: As soon as enough binder is deposited to form interparticle bridges, strength develops following an exponential course, followed by a saturation range where the additional binder cannot contribute much more to the strength of the binder bridges.[28,32,33]

The **abrasion resistance** of the printed parts was measured to get a better understanding of the ability of the samples to withstand scratching or wear caused by friction during handling and casting. Figure 10 compares the abrasion resistance of the 3D-printed sintered bauxite samples with a catalyst content of 0.4 wt.-% and a recoating speed of 200 mm/s with samples printed with GS14 using a catalyst content of 0.2 wt.-% and a recoating speed of 100 mm/s. As expected, the abrasion resistance increases with higher binder amounts. For CastBall, the abrasion resistance was measured to be higher than the reference material, and as high as 43 at the standard binder amount whereas silica sand only showed an abrasion resistance number of 20. Even if scratch hardness testing is a standard method in the testing of molding materials, this dimensionless comparative value is difficult to interpret. However, a higher abrasion resistance value indicates that handling of the printed parts will be facilitated and sand abrasion during casting may be reduced.

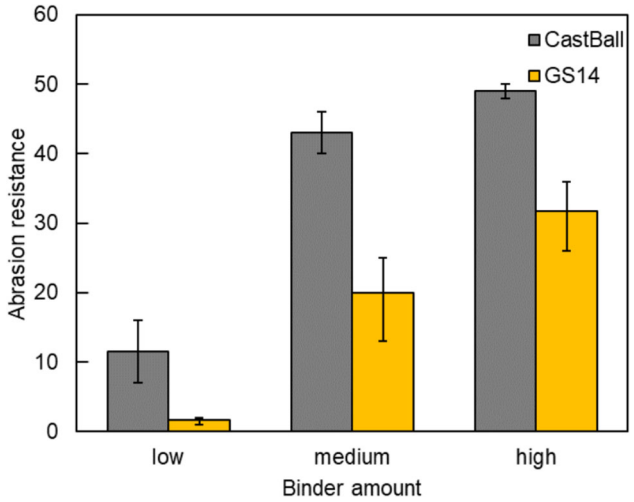

***Figure 10. Comparison of the abrasion resistance of CastBall premixed with a catalyst amount of 0.4 wt.-% and recoated at a recoating speed of 200 mm/s, and GS14 RP premixed with 0.2 wt.-% catalyst and recoated with 100 mm/s. Number of samples* n=2.**

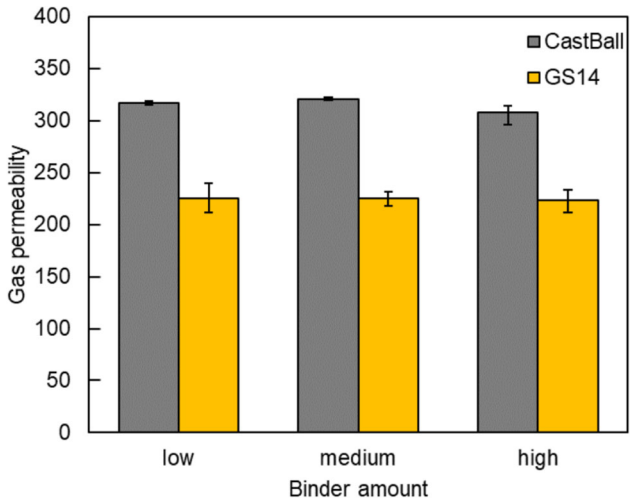

***Figure 11. Comparison of the gas permeability of CastBall premixed with a catalyst amount of 0.4 wt.-% and recoated at a recoating speed of 200 mm/s, and GS14 RP premixed with 0.2 wt.-% catalyst and recoated with 100 mm/s. Number of samples* n=[2;3].**

Figure 11 compares the **gas permeability** of CastBall and GS14 samples. A higher gas permeability can lead to reduced gas defects and metal oxides in the melt, which is an advantage for casting processes. Both systems reveal that the amount of binder does not have a decisive influence on gas permeability. In a previous study,[34] a correlation was identified between the quantity of binder and gas permeability. However, this correlation was found to be associated with density.[34] It is shown that specimens printed from CastBall have, with an average of 315, a higher gas permeability than GS14 specimens. While the GS14 parts have an average permeability of 224, the permeability values of CastBall are on the same scale as the

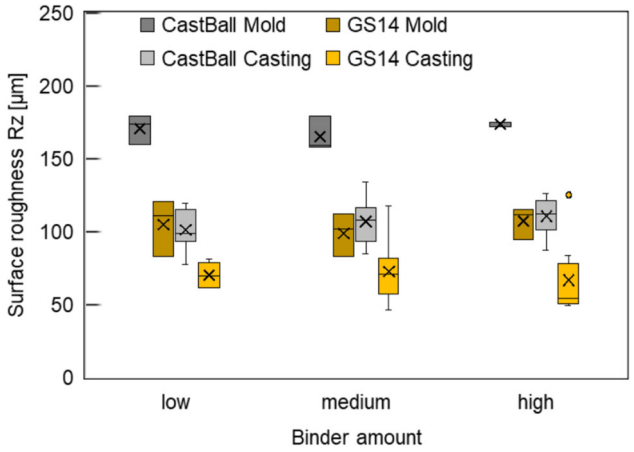

***Figure 12. Comparison of the mean roughness depth* R_z *of 3D-printed samples. CastBall: premixed with a catalyst amount of 0.4 wt.-% and recoated at a recoating speed of 200 mm/s. GS14 RP: premixed with 0.2 wt.-% catalyst and recoated with 100 mm/s. Number of samples mold:* n=3, *casting:* n=9.**

sintered mullite sand Cerabeads ES 650 which has comparable particle sizes and morphologies and would thus be an interesting material benchmark system for future studies. The higher gas permeability compared to GS14 is mainly attributed to the difference in particle size of the two different sands. However, the round grain shape may also contribute to improved gas transport.

Figure 12 shows the **surface roughness** R_z for the printed molds and aluminum castings, measured in plane, and plotted in dependence of the binder content. Samples 3D printed with CastBall show a generally higher mean roughness depth R_z of around 170 µm, which is attributed to the larger grain sizes of the sand. The surface roughness values of all samples demonstrate minor variations in relation to the quantity of binder employed. The surface roughness of the samples with GS14 is found to be around 104 µm. The surface quality of the mold influences the surface quality of the casted part but the mean roughness depth is known to be lower for the casting due to wetting effects. This is confirmed in Figure 12 in the measurements perpendicular to the printing direction. The effect of the printing direction on the surface roughness as characterized systematically for a silica sand system similar to GS14 by Bedel et al.[35] is not part of this study, but could be of interest in future works.

An interesting aspect worth noting is the observed slower response to a finishing treatment by air blasting for CastBall compared to GS14RP, which might be attributable to the higher catalyst addition. Since the differences were not significantly pronounced, further investigations with a larger sample size would provide a more definitive understanding. Moreover, future studies may assess also the wear and tear on 3D printing equipment that may be

increased by excessive use of catalyst or the material hardness despite the particles' beneficial shape.

Sand cores with medium binder content from quartz and bauxite sand are printed, placed into a 3D-printed casting mold from GS14RP, and cast with the aluminum alloy AlSi7Mg0.3 at a pouring temperature of 750 °C. Figure 13a displays a close-up of the bauxite sand core. The inner structure of the casting is a disk with a diameter of approx. 180 mm and a minimum thickness of 8 mm.

Bauxite sand is found to be slightly easier to decore after casting in identical molds (Figure 13b) although the strength of the sand cores was found to be higher (Figure 9). However, an increase in the presence of sand inclusions has been observed on the surface that was in contact with the bauxite sand core (Figure 13c, e) compared to the same casting made with a silica sand core (Figure 13d, f). The reason might be the coarser grain diameter: the sand grains that are spaced further apart and may be enclosed more easily by the melt. However, since sand inclusions are also found in the silica sand casting, the inclusions of bauxite sand may only appear more conspicuous because of the dark color and the actual reason for the inclusions is the sand mold and casting system design having a vertical parting line. When inserting the cores in the sand mold, sand may rub off from the sharp edge of the support visible in Figure 13a. Even so, the resistance against abrasion of the melt needs to be subject of further investigations since improved abrasion resistance for sand cores printed with bauxite sand was found during mold material characterization (Figure 10). The surface roughness R_z in the inner structure of the pump housing casting is measured to be in average 108 µm and thus aligns well with the previous measurements in plane (Figure 12).

Concluding Remarks

This research has revealed new possibilities for the application of sintered bauxite sand in the field of 3D printing of casting molds and cores. Specifically, it has been demonstrated that bauxite sand can be effectively processed through binder jetting using the most widely employed furan binder. In addition to the beneficial material properties known from the state of the art, such as improved decoring behavior, low thermal expansion, and high-temperature stability, the findings of this study demonstrate that sintered bauxite sand exhibits a substantial advantage in terms of processing time in binder jetting, with the capacity to double the recoating speed in comparison with silica sand. Additionally, it was determined that sintered bauxite sand tends to demonstrate higher strengths when an increased catalyst content is employed, which could lead to its use in complex high-quality cast products.

It was found that compared to silica sand printing, increased catalyst contents are needed which can present several challenges related to the use of sulfonic acid as the catalyst. This is of particular concern in the context of a transition toward greener production, as increased catalyst usage might result in elevated emissions during casting, thereby contributing to even more extensive workplace pollution. Holtzer et al. found that the hardener is decisive for the formation of substances from the PAHs group (polycyclic aromatic hydrocarbons) and PAHs emissions from molding sands decrease with lower concentrations of p-toluenesulfonic acid.[36] Exposure to PAHs is considered a severe health risk, particularly in relation to cancer.[37] With regard to safety, it would thus be advisable to, at least, use other types of hardeners to avoid further increasing the health risks of handling these already critical chemicals, Phenolic resin is often used in 3D printing as a thermal curing system and is estimated to be less sensitive to the pH value of the sand. Since phenolic resin is also resistant to hot deformation, it would be predestined for advanced applications where thin structures inside components made of high-temperature casting materials, e.g., hydraulic blocks, are required. A very high potential is attributed to the use of environmentally friendly inorganic silicate binders. Here, the advantageous decoring behavior can be particularly beneficial and, in combination with the physical–chemical reaction during the curing of water glass, the higher pH value of sintered bauxite sand compared to silica sand could even be an advantage.

The biggest hurdle of the wider use of sintered bauxite sand is the higher cost which is estimated to be 5 to 10 times higher than that of silica sand. Given that each ton of iron or steel casting typically requires 1 ton of foundry sand during its production,[38] the reclamation of sand is of environmental, cost, and logistical importance. Studies on the reclamation of bauxite sand processed in 3D printing machines thus need to be carried out in order to quantify the material flows and estimate the cost structure, which depends largely on its reusability over many casting cycles. In terms of energy consumption and CO2 emissions, clear technological benefits in the casting product and the sand's reusability are crucial to leverage the environmental impact of the energy-intensive sintering process of bauxite sand. Further lifecycle assessment studies are needed for a comprehensive evaluation of the overall emissions. Noteworthy is the fact that silica sand has a much lower attrition resistance when compared to the sintered bauxite sand, which causes high generation of fines and suspended dust in the workplace, a problem that is exacerbated by the presence of free crystalline silica. This implies environmental, occupational health and financial issues, as foundries are required to implement and maintain engineering and personal protective measures to minimize risks. Furthermore, the lower silica thermal stability, sometimes,

Figure 13. (a) Close-up of a pump housing core printed with sintered bauxite sand. (b) Casting of pump housing including casting system. Cut-open pump housing cast with sintered bauxite sand (c) and silica sand (d). Micrograph of a bauxite (e) and silica (f) sand inclusion.

results in castings with low dimensional stability and greater potential for defects, such as veining, metal penetration, hot cracks, and scabs. Between this and that, sintered bauxite sands can be a cost-efficient sand of choice for foundries if sand reuse strategies are implemented to overcome the initial material cost barrier.

Acknowledgments

We would like to express our sincere gratitude to Mr. Écio Rodrigues Araújo and Mr. Luiz Ricardo Curimbaba from the Curimbaba Group for their valuable contributions and expertise, which played a crucial role in the execution of this research.

Funding

Open Access funding enabled and organized by Projekt DEAL.

REFERENCES

1. P. Erhard, C. Hartmann, R. Li, W. Volk, D. Günther, Advanced procedures for series production with 3D-printed core packages. Int. J. Metalcast. **17**(4), 2572–2583 (2023). https://doi.org/10.1007/s40962-023-01046-1
2. S.R. Sama, T. Badamo, G. Manogharan, Case studies on integrating 3D sand-printing technology into the production portfolio of a sand-casting foundry. Int. J. Metalcast. **14**(1), 12–24 (2020). https://doi.org/10.1007/s40962-019-00340-1
3. P. Lynch, C.R. Hasbrouck, J. Wilck, M. Kay, G. Manogharan, Challenges and opportunities to integrate the oldest and newest manufacturing processes: metal casting and additive manufacturing. Investig Fluid Flow During Recoat Process Addit Manuf **26**(6), 1145–1154 (2020). https://doi.org/10.1108/RPJ-10-2019-0277
4. R. Kleinhans, M. Pintore, P. Erhard, R. Renz, J. Tesfu, Thermal properties of 3D-printed molds for light metal casting. Int. J. Metalcast. (2024). https://doi.org/10.1007/s40962-024-01411-8
5. H. Yang, Z. Shan, D. Yan, J. Shi, H. Shi, J. Huang, Advances in digital multi-material composite sand-mold binder-jetting forming technology and equipment. Addit Manuf Front **3**(2), 200138 (2024). https://doi.org/10.1016/j.amf.2024.200138
6. IARC Working Group on the Evaluation of Carcinogenic Risks to Humans, International Agency for Research on Cancer, World Health Organization, "A review of human carcinogens," International Agency for Research on Cancer, Lyon (2012).
7. Occupational Safety and Health Administration, "National Emphasis Program—Respirable Crystalline Silica," OSHA Instruction, CPL 03-00-023 (2020), https://www.osha.gov/sites/default/files/enforcement/directives/CPL_03-00-023.pdf (March 5, 2025).
8. Occupational Safety and Health Administration, "Small Entity Compliance Guide for the Respirable Crystalline Silica Standard for for General Industry and Maritime," OSHA 3911-12 (2023), https://www.osha.gov/sites/default/files/publications/OSHA3911.pdf (March 5, 2025).
9. M. Casting, OSHA's crystalline silica rule: OSHA's crystalline silica rule: what should your foundry be doing now? Mod. Cast. **10**, 30–34 (2017)
10. U. Recknagel, M. Dahlmann, Spezialsande: formgrundstoffe für die moderne kern- und formherstellung. Giesserei-Praxis **11**, 1–7 (2010)
11. A.L. Pereira, E.C. Carlini, L.L.H.C. Ferreira, P.M. Nakachima, R.V. Fernandes, "Estudo do Comportamento Térmico de Misturas de Areia Cerâmica Sinterizada à Base de Bauxita com Areias de Sílica e Cromita," *20°Congresso Nacional de Fundição—CONAF/ABIFA* (2024).
12. A.L. Pereira, C. Silva, E.C. Carlini, E. Sousa, L.L.H.C. Ferreira, P.M. Nakachima, R.V. Fernandes, "Comparativo entre diferentes Tipos de Areias quanto à sua Durabilidade Térmica e Física, visando sua recuperação em uma Fundição," *19°Congresso Nacional de Fundição—CONAF/ABIFA* (2022).
13. S. Ramrattan, L.L.H.C. Ferreira, A.L. Pereira, P.M. Nakachima, "Effects of Thermo-Mechanical Anisotropy in 3D Printed Silica and Ceramic Sands Disc-Shaped Specimens," *20°Congresso Nacional de Fundição—CONAF/ABIFA* (2024).
14. A.L. Pereira, M.A. Reis, L.L.H.C. Ferreira, P.M. Nakachima, Brazilian refractory grade bauxite: a new alternative to refractories makers and users. Cerâmica **65**(suppl 1), 40–46 (2019). https://doi.org/10.1590/0366-6913201965S12611
15. A. Mostafaei, A.M. Elliott, J.E. Barnes, F. Li, W. Tan, C.L. Cramer, P. Nandwana, M. Chmielus, Binder jet 3D printing—Process parameters, materials, properties, modeling, and challenges. Prog. Mater. Sci. **119**, 100707 (2021). https://doi.org/10.1016/j.pmatsci.2020.100707

16. Q. Chen, E. Juste, M. Lasgorceix, F. Petit, A. Leriche, Binder jetting process with ceramic powders: Influence of powder properties and printing parameters. Open Ceram **9**, 100218 (2022). https://doi.org/10.1016/j.oceram.2022.100218
17. B. Utela, D. Storti, R. Anderson, M. Ganter, A review of process development steps for new material systems in three dimensional printing (3DP). J. Manuf. Process. **10**(2), 96–104 (2008). https://doi.org/10.1016/j.jmapro.2009.03.002
18. D. Schulze, *Powders and bulk solids: Behavior, characterization, storage and flow* (Springer, Berlin, 2008)
19. S. Vock, B. Klöden, A. Kirchner, T. Weißgärber, B. Kieback, Powders for powder bed fusion: a review. Prog Addit Manuf **4**(4), 383–397 (2019). https://doi.org/10.1007/s40964-019-00078-6
20. S. Diener, A. Zocca, J. Günster, Literature review: Methods for achieving high powder bed densities in ceramic powder bed based additive manufacturing. Open Ceram **8**, 100191 (2021). https://doi.org/10.1016/j.oceram.2021.100191
21. Strobel Quarzsand GmbH, "GS14 RP," http://www.strobel-quarzsand.de/media/GS14RP.pdf (2025).
22. F. Ettemeyer, P. Lechner, T. Hofmann, H. Andrä, M. Schneider, D. Grund, W. Volk, D. Günther, Digital sand core physics: Predicting physical properties of sand cores by simulations on digital microstructures. Int. J. Solids Struct. **188–189**, 155–168 (2020). https://doi.org/10.1016/j.ijsolstr.2019.09.014
23. American Foundry Society, "Mold & Core Test Handbook," American Foundry Society (AFS (2019).
24. G. Miao, M. Moghadasi, W. Du, Z. Pei, C. Ma, Experimental investigation on the effect of roller traverse and rotation speeds on ceramic binder jetting additive manufacturing. J. Manuf. Process. **79**, 887–894 (2022). https://doi.org/10.1016/j.jmapro.2022.05.039
25. G. Miao, W. Du, Z. Pei, C. Ma, A literature review on powder spreading in additive manufacturing. Addit. Manuf. **58**, 103029 (2022). https://doi.org/10.1016/j.addma.2022.103029
26. T.P. Thaba, K.D. Nyembwe, Thermal reclamation of used sand produced by binder jetting processes. MATEC Web Conf **388**, 9001 (2023). https://doi.org/10.1051/matecconf/202338809001
27. D. Günther, F. Mögele, "Additive Manufacturing of Casting Tools Using Powder-Binder- Jetting Technology," In: Shishkovsky, I.V., editor, New Trends in 3D Printing, InTech (2016).
28. H.-J. Son, S. Jang, H.-J. Hyeon, H.-J. Lee, J.-J. Yang, B.-Y. Park, S.-S. Gwak, S.-W. Jang, C.-J. Bae, Mechanical integrity and erosion resistance of 3D sand printing materials. Mater. Des. **233**, 112204 (2023). https://doi.org/10.1016/j.matdes.2023.112204
29. N. Anwar, T. Sappinen, K. Jalava, J. Orkas, Comparative experimental study of sand and binder for flowability and casting mold quality. Adv. Powder Technol. **32**(6), 1902–1910 (2021). https://doi.org/10.1016/j.apt.2021.03.040
30. D. Günther, P. Erhard, S. Schwab, I. Taha, 3D Printed Sand Tools for Thermoforming Applications of Carbon Fiber Reinforced Composites-A Perspective. Materials **14**(16), 4639 (2021). https://doi.org/10.3390/ma14164639
31. #3DBenchy, "#3DBenchy—A Small Giant in the World of 3D Printing," 2017, https://www.3dbenchy.com/3dbenchy-a-small-giant-in-the-world-of-3d-printing/ (February 11, 2025).
32. S.I. Yanez-Sanchez, M.D. Lennox, D. Therriault, B.D. Favis, J.R. Tavares, Model Approach for Binder Selection in Binder Jetting. Ind. Eng. Chem. Res. **60**(42), 15162–15173 (2021). https://doi.org/10.1021/acs.iecr.1c02856
33. P. Erhard, V.T. Tanjavooru, C. Hartmann, L. van den Bosch, A. Seidel, W. Volk, D. Günther, Simulation of Binder Infiltration in Additive Manufacturing of Sand Molds. Adv. Eng. Mater. **25**(20), 2300212 (2023). https://doi.org/10.1002/adem.202300212
34. D. Martinez, C. Bate, G. Manogharan, Towards functionally graded sand molds for metal casting: engineering thermo-mechanical properties using 3D sand printing. JOM **72**(3), 1340–1354 (2020). https://doi.org/10.1007/s11837-019-03975-x
35. M. Bedel, A. Fabre, N. Coniglio, Defining the printing direction impact of additively manufactured sand molds on casting roughness. J. Manuf. Process. **116**, 329–340 (2024). https://doi.org/10.1016/j.jmapro.2024.02.068
36. M. Holtzer, A. Kmita, S. Żymankowska-Kumon, A. Bobrowski, R. Dańko, Influence of the hardener on the emission of harmful substances from moulding sands with furan resin in the pyrolysis process. Arch. Foundry Eng. **16**(1), 107–111 (2016). https://doi.org/10.1515/afe-2016-0012
37. C. Blanco-Alegre, A.I. Calvo, M. Castro-Sastre, A.I. Fernández-Abia, P. Rodríguez-González, F. Oduber, A. Castro, J. Barreiro, R. Fraile, Analysis of gaseous emission and particle number size distributions in metal casting processes with binder jetting moulds. Build. Environ. **252**, 111297 (2024). https://doi.org/10.1016/j.buildenv.2024.111297
38. C. Anderson, Recycling of Foundry Sand Through Chemical and Physical Beneficiation, 2010, Center for Resource, Recovery & Recycling Inaugural Meeting, Boston. https://doi.org/10.13140/RG.2.2.25260.26247 .